

Membrane fluctuations and acidosis regulate cooperative binding of “Marker of Self” CD47 with macrophage checkpoint receptor SIRP α

Jan Steinkühler^{1,2}, Bartosz Różycki³, Cory Alvey¹, Reinhard Lipowsky², Thomas R. Weikl², Rumiana Dimova², and Dennis E. Discher^{1*}

¹ Molecular & Cell Biophysics Lab, University of Pennsylvania, Philadelphia, 19104 PA, USA

² Theory and Bio-Systems, Max Planck Institut of Colloids and Interfaces, Science Park Golm, 14424 Potsdam, Germany

³ Institute of Physics, Polish Academy of Sciences, Al. Lotników 32/46, 02-668 Warsaw, Poland

Abstract

Cell-cell interactions that result from membrane proteins binding weakly in *trans* can cause accumulations in *cis* that suggest cooperativity and thereby an acute sensitivity to environmental factors. The ubiquitous “marker of self” protein CD47 binds weakly to SIRP α on a macrophage, which leads to accumulation of SIRP α at a phagocytic synapse and ultimately to inhibition of engulfment of ‘self’ cells – including cancer cells. We reconstituted this macrophage checkpoint with CD47-GFP displayed on giant vesicles generated from plasma membranes and then imaged vesicles adhering to SIRP α immobilized on a surface. CD47 diffusion is impeded near the surface, and the binding-unbinding events reveal cooperative interactions as a concentration-dependent, two-dimensional affinity. Membrane fluctuations link cooperativity to membrane flexibility with suppressed fluctuations in the vicinity of bound complexes. Slight acidity (pH=6) stiffens membranes, diminishes cooperative interactions, and also reduces ‘self’ signaling of cancer cells in phagocytosis. Sensitivity of cell-cell interactions to microenvironmental factors – such as the acidity of tumors and other diseased or inflamed sites – can thus arise from collective, cooperative properties of membranes.

* Correspondence: discher@seas.upenn.edu

Keywords: adhesion, vesicles, elasticity, cooperative binding, GPMV

Introduction

Cells use adhesion molecules to interact with and thereby *identify* other cells, but recent theoretical and simulation results indicate the physical act of binding is highly cooperative and mediated by membrane fluctuations in a generalized law of mass action (Krobath_et_al.,2009). Differences in 3D versus 2D binding have been studied with cells adhering to supported lipid bilayers (Zhu_et_al.,2007; Tolentino_et_al.,2008) and with lipid vesicles bearing reconstituted binding molecules (Fenz and Sengupta, 2012; Bihl_et_al.,2014, Chan_et_al.,2007), but cell experiments are complicated by cytoskeleton-driven remodeling (Huppa_et_al.,2010) and liposomes lack a molecular richness of cell membranes. Here we use cell-derived giant vesicles that lack cytoskeletal interactions (Sezgin_et_al.,2012), and we focus on universally expressed protein CD47 in membranes as it mediates adhesion to SIRP α on a rigid surface. Wide-ranging (bio)physical experiments provide evidence of equilibration and are linked closely to multiscale simulation.

CD47 binding to SIRP α on macrophages ultimately inhibits engulfment of “self” cells by macrophages and is now being pursued clinically in cancer therapy by antibody-blockade of this ‘macrophage checkpoint’ (Seiffert_et_al.,1999; Oldenborg_et_al.,2000; Vernon-Wilson_et_al.,2000; Alvey and Discher, 2017). ‘Self’ cells also signal to T-cells (via PDL1 interactions with PD1) through a phosphatase pathway shared by SIRP α , and antibody-blockade of the PDL1-PD1 T-cell checkpoint has already proven surprisingly effective in the clinic against some cancers. As with the majority of cell-cell signaling molecules, *trans* interactions of two integral membrane proteins in juxtaposed plasma membranes leads to a dependence of membrane adhesion on membrane conformation. An unfavorable membrane geometry such as with chemically rigidified discocyte-shaped red blood cells, limits CD47 signaling and leads to efficient phagocytosis of the blood cells (Sosale_et_al.,2015a). For distances between membranes that are similar to the sizes of adhesion molecules, the membrane-membrane interaction depends on (membrane) flexibility and shape fluctuations as well as conformations of binding molecules (Xu_et_al.,2015). Studies here of a native membrane protein interacting with its immobilized receptor provides – more generally – some of the first experimental evidence of cooperative binding due to suppression of

membrane fluctuations. The findings should apply to immunological synapse complexes and many membrane bound signaling complexes beyond CD47-SIRP α at the phagocytic synapse.

Results and Discussion

Cell-derived vesicles retain CD47 and thermally fluctuate

Membrane sheets of several hundred μm^2 in area detach from the cortical cytoskeletons of CD47-GFP expressing HEK cells (**Fig.1A-left**) by a method previously used to study lipid segregation (Sezgin_et_al.,2012). These sheets spontaneously bud and seal to form giant unilamellar vesicles that are more specifically referred to as giant plasma membrane vesicles (GPMVs). GPMVs possess a near native composition of lipid and membrane protein (Bauer_et_al.,2009) and retain lipid and protein mobility and conformation (Baumgart_et_al.,2007; Sezgin_et_al.,2012; Veatch_et_al.,2008) as well as optically resolvable shape fluctuations (**Fig.1B-right inset**).

Phase contrast microscopy with μs -exposure times shows the amplitudes of Fourier modes q of membrane fluctuations at the equatorial plane (**Fig.1B**). The q^{-3} dependence agrees with Helfrich theory of elastic membranes as previously applied to pure lipid vesicles in a fluid state (Gracia_et_al.,2010; Lipowsky,1991). GPMV mechanical properties can thus be reduced to a few parameters such as bending rigidity, tension, and preferred curvature that integrate out detailed molecular composition and biological state(s) of membranes.

CD47 is properly oriented in GPMVs and functional for binding

CD47-GFP make GPMVs uniformly fluorescent (**Fig.1A,S1A**), but to understand if CD47 is properly orientated, we added a red-fluorescent anti-CD47 that binds CD47's extracellular domain. The two signals correlate (**Fig.1C**) and confirmed a natural cell-cell variation of CD47 levels between GPMVs. A range of CD47 concentrations could thus be studied in adhesion.

To assess CD47-SIRP α binding, we physisorbed the extracellular domain of SIRP α (fused to a large single domain protein, GST) or else the surface-blocking agent bovine serum albumin (BSA) on coverslips (Subramanian_et_al.,2006). SIRP α homogenously adsorbed based on fluorescence imaging (**Fig.S1B**). Gravitational settling of GPMVs onto BSA-coverslips showed near-spherical vesicle shapes and therefore little interaction (**Fig.1A,right-top**). On SIRP α -coverslips in contrast, GPMVs deform strongly as they adhere

(Fig.1A,right-bottom): the upper unbound cap is spherical whereas the flattened lower membrane segment is where CD47 accumulated in binding the immobilized SIRP α (**Fig.1A,plot**). After initial contact between a GPMV and the SIRP α surface, CD47-GFP diffused into the adhesion zone in a ring-like fashion and became homogeneous over time (**Fig.S1C**). Experiments were then done on GPMVs with equilibrated and homogenous adhesion, lacking any domain formation and thus implying a single species of CD47-SIRP α adhesion complexes (Weikl_et_al.,2009). Diffusion dynamics in these two segments were measured by fluorescent recovery after bleaching (FRAP) of μm -sized spots.

2D binding affinity determined from FRAP

FRAP dynamics in small bleached spots differed between unbound and bound membrane segments. In unbound segments, CD47 fluorescence recovers over seconds and yields a diffusion constant of $D_{\text{cd47}}=0.12 \pm 0.02 \mu\text{m}^2/\text{s}$ ($n=3$) as determined from fitting to a standard model for unhindered diffusion (Soumpasis, 1983). In stark contrast, CD47 within the adherent zone recovers ~ 100 -fold slower (**Fig.1D**). CD47-SIRP α unbinding events are likely followed by a short distance of free diffusion before re-binding (Sprague_et_al.,2004). Such trajectories are governed by a reaction-diffusion model ((Sprague_et_al.,2004); Material and Methods). By fitting the model to the measured time-intensity traces the 2D binding affinity $[R]K_{2D}=[R]k_{\text{on}}/k_{\text{off}}$ is extracted. Here, $[R]$ is the density of (unbound) SIRP α on the glass surface. The fit to the model is satisfactory and we obtain $[R]K_{2D}$ data for individual vesicles expressing different CD47 densities. The results are independent of the exact value of $[R]$, but $[R] \approx 4000$ molecules/ μm^2 , see **Fig.S1B**). Strikingly, CD47-SIRP α complex concentration and binding affinity are positively correlated, indicative of cooperative binding (**Fig.2A**). Computer simulations help clarify cooperative effects in CD47-SIRP α binding and unbinding.

Cooperative binding by suppression of membrane fluctuations

Our multi-scale modeling approach combines (i) simulations of a coarse-grained CD47-SIRP α complex (**Fig.2B**) to determine the effective spring constant of the complex, and (ii) simulations of large membrane segments adhering via CD47-SIRP α complexes, modeled as elastic springs (**Fig.2B,C**). In simulations of a CD47-SIRP α complex, CD47's transmembrane domain is embedded in a small membrane patch parallel to the substrate and connected by

a short flexible linker to CD47's extracellular domain. This domain is bound to SIRP α in the correct orientation based on the crystal structure of the complex (PDB-file 2JJS). SIRP α is connected via a linker to substrate-bound GST per experiments. Flexible linkers and protein interactions per (Kim and Hummer, 2008) have been successfully applied to several multi-protein complexes, including ERK2-HePTP (Francis_et_al.,2011) and ESCRT complexes (Boura_et_al.,2011, Boura_et_al.,2012). Variation of the separations between the membrane patch and substrate observed in simulations (**Fig.S2**) result from molecular architecture and flexibility of the CD47-SIRP α complex. The mean $l_0=17.2$ nm of these separations is the preferred membrane-substrate separation of the complex, and the standard deviation $\sigma=1.2$ nm reflects flexibility and an effective spring constant $k_s=k_B T/\sigma^2$ of the complex.

In our simulations of large adhering membrane segments (**Fig.2C,D**), membranes are elastic surfaces with bending rigidity $\kappa=10k_B T$, as measured experimentally, and discretized into quadratic patches of size 15×15 nm² (Weikl and Lipowsky,2006). Membrane patches that contain CD47-SIRP α complexes are bound to the substrate with separation l_0 and spring constant k_s . Repulsive interactions between the protein layer on the substrate and the membrane are taken into account by allowing only local separations $l>(l_0-\Delta l)$ between membrane patches and substrate, with $\Delta l>0$. From simulations, we obtain distributions $P(l)$ of local separations that depend on concentration [RL] of CD47-SIRP α complexes (**Fig.2C**) because bound complexes constrain membrane shape fluctuations reflected by $P(l)$.

From the distributions $P(l)$, and from the preferred length l_0 and spring constant σ of the complexes, we obtain the binding constant K_{2D} from (Xu_et_al.,2015)

$$K_{2D} = \int \hat{K}_{2D}(l)P(l)dl$$

with $\hat{K}_{2D}(l) = K_{\max} \exp[-(l - l_0)^2/\sigma^2]$ up to a prefactor K_{\max} , which we treat as a fit parameter. K_{2D} increases with bond concentration [RL] (**Fig.2A**), because distributions $P(l)$ become narrow and shift towards l_0 with increasing [RL] (**Fig.2E**). Modeling results agree with experimental datapoints for different values of Δl for the repulsion between membrane and protein-coated substrate (**Fig.2A**). We vary Δl because neither the thickness of protein layers nor the role(s) of GPMV proteins in steric repulsion are known. Strong increase of K_{2D} with [RL] reflects cooperative binding of CD47-SIRP α , which results from smoothing of membrane fluctuations by bound complexes (Krobath_et_al.,2009; Hu_et_al.,2013). Smoothing facilitates formation of additional CD47-SIRP α complexes.

Slight acidity inhibits CD47-SIRP α cooperativity and favors phagocytosis

To further validate our model, we explored effects of membrane fluctuations (and hence cooperativity) in relation to the bending rigidity of the membrane. We discovered that subjecting cells to a slight acidity of pH=6 induces stiffening of the GPMV (**Fig.3A**). In both simulations and experiment, such rigidification led to a substantial decrease in cooperativity (**Fig.3B**). Simulation and experiment are linked *via* the measured bending rigidity, which lumps the complex cell (plasma membrane) response to a pH change into a single parameter. Absolute values of $[R]K_{2D}$ data points are also significantly reduced, as confirmed by an independent but more approximate determination of K_{2D} using fluorescent intensities of adherent and free membrane segments (**Fig.3C**). Some alternative explanations for the decreased 2D binding affinity can be ruled out by further experiment: First, binding of soluble SIRP α to red blood cells does not exhibit a strong pH dependence in the 3D binding affinity (**Fig.S3A**). Secondly, density changes in absorbed protein $[R]$ do not change with pH, perhaps because of a change in conformational and rotational free-energy loss of CD47 and/or SIRP α during binding (Xu_et_al.,2015). Regardless of the exact cause of the two-to-four fold decrease in 2D binding affinity with decreased pH, the loss of cooperativity is likely to be more important to signaling, because CD47 densities vary over 1-2 orders of magnitude across otherwise healthy cells and yet CD47 signaling remains effective (Subramanian_et_al.,2007). Changes in CD47's collective binding affinity for SIRP α could ultimately inhibit a cell's ability to efficiently signal through this pathway.

Tumor tissues commonly experience acidosis (Tannock and Rotin,1989). Opsonization of a Lung cancer derived cells (A549) with an IgG to present an "eat me" signal to macrophages normally does not efficiently engage phagocytosis due to expression of CD47 on the cancer cell surface (Sosale_et_al.,2015b). However, opsonization under acidic conditions caused an increase in phagocytosis (**Fig.4A**), consistent with the biophysical data showing diminished cooperativity and binding capacity of CD47 at slightly acidic conditions of pH 6 (**Fig.3B,C**). When A549 cancer cells are cultured long-term at pH=6, CD47 levels are elevated (**Fig.4B**), indicating a cellular signaling cascade that works against reduction in "self" signaling by upregulation of CD47. Together this data suggest that the measured two

dimensional binding affinities reveal physiologically relevant parameters that would have been missed in classic binding affinity assay.

Conclusion

Here, we have studied protein complex formation on reconstituted, cytoskeleton-free, plasma membrane and demonstrated that membrane shape fluctuations on nanoscales lead to cooperative binding. In contrast to our plasma membrane vesicles, cellular plasma membranes are bound to a cytoskeleton that confines shape fluctuations on length scales larger than the cytoskeletal mesh size (~50-100 nm) (Morone_et_al.,2006), but hardly affects fluctuations on lateral scales of tens of nm's (typical distance between neighboring bound complexes) that lead to cooperative binding (Weigl et al, 2009; Hu et al, 2013). Therefore, these nanoscale thermal fluctuations and, thus, the binding cooperativity should persist in living cells. Cell membrane fluctuations appear to be driven by active processes and by thermal motion (Biswas_et_al.,2017; Turlier_et_al.,2016; Monzel_et_al.,2015), and both can enhance binding cooperativity. In general, fluctuations and displacements of single, unbound membranes should be distinguished from distance fluctuations between two membranes adhering via protein complexes (Lipowsky,1995). The distance fluctuations of two adhering membranes or of one membrane adhering to a surface are constrained by the protein complexes on length scales larger than the typical distance between neighboring complexes, which leads to binding cooperativity. (**Fig.2**). GPMVs are known to exhibit many aspects of native cell membranes, and yet the membrane mechanical properties can be described using a just few parameters that connect experiment to theory and simulation. Membrane fluctuations are reduced when the plasma membrane is stiffened by a pH shift to pH 6, which can be induced by tumor tissue acidosis (**Fig.3**) (Tannock and Rotin,1989). Consistently between experiments on plasma membrane vesicles, multiscale simulation and phagocytoses experiments we find reduced CD47 signaling (**Fig.4A**). Clearly, enhanced phagocytoses at pH 6 does not have to be caused exclusively by the demonstrated diminished CD47 (K_{2d}) binding affinity. However, the here presented model system can be used to address the contribution to total cell signaling from binding affinities of individual signaling components in absence of the cytoskeleton, while presenting a physiological, membrane bound, environment. Finally we speculate that that reduction in CD47 signaling by membrane rigidification selects for the

elevated levels of CD47 in many tumors . Reduction of CD47 signaling would otherwise tend to enhance phagocytosis.

Reductionist approaches to cell adhesion with giant vesicles derived from plasma membranes provide, more generally, attractive models of cytoskeleton-independent adhesion that can be thermodynamically equilibrated. CD47 remains integrated, properly oriented, and functional in plasma membrane derived vesicles. A theoretical prediction of cooperative binding and hence a non-linear law of mass action is confirmed through studies of the interaction of CD47 to its cognate ligand SIRP α . We also varied membrane bending rigidity of extracted plasma vesicles. Our multiscale simulation and experimental approaches identify a few intuitive parameters, which describe binding, unbinding and cooperative effects for a wide range of membrane bound complexes. Binding and signaling in cell-cell interactions are not only determined by the relative affinity of the complexes but also indirectly by changes such as the membrane fluctuation spectrum. Our method of reconstituted adhesion should have many applications where affinities of cell signaling complexes are investigated. Ultimately, convolution of membrane fluctuations with binding of adhesion molecules provides an elegant way to control activation and clustering for cell signaling.

Material and Methods

Cell line authentication and contamination testing CD47-GFP HEK 293 and A549 cell lines were authenticated and screened for contamination using American Type Culture Collection (ATCC) standards, Tech Bulletin number 8 (TB-0111-00-02; yr 2010). HEK 293 and A549 cell lines were acquired from ATCC.

GPMV Isolation Before experiments, CD47-GFP HEK cells (see Supplemental Methods) were plated under identical conditions in T-25 culture flasks and cultured for 3 days until cells were 90% confluent. GPMVs were isolated according to the protocol (Sezgin_et_al.,2012). HEK cells were incubated with 2mM DTT, 25mM PFA at 37°C for 1 hour. For experiments at varying pH, the GPMV buffer was adjusted to the desired pH at the day of the experiment.

Purification and absorption of SIRP α on glass slides The soluble extracellular domain of SIRP α was purified as previously described (Seiffert_et_al.,1999). The resulting protein was tagged by GST and we refer to the resulting SIRP α Ex-GST as to “SIRP α ”. SIRP α at a concentration of 34nM was then incubated on cleaned glass slides (2x rinsing with ethanol and ultra-pure water or five minutes' exposure to oxygen plasma yielded the same results) for one hour in phosphate buffered saline solution at room temperature. Unbound SIRP α was washed away and uncovered glass surface was blocked by incubation with 1% BSA, 0.05% Tween-20 for one hour at RT. The coated glass slides were then washed in GPMV buffer at the desired pH and immediately covered with GPMV suspension.

Confocal imaging, FRAP experiments and image analysis Confocal images were obtained on a Leica SP8 system, dyes were excited using the 488 and 638 laser lines and fluorescence was collected (495-600nm and 650-750nm). To avoid cross-talk between the channels, two-color images were always obtained sequentially. FRAP experiments were performed on the same system. A circle of 1 μ m in diameter was bleached using the 488 laser for two consecutive frames and recovery was observed under normal imaging conditions for 60 frames and 0.2 frames per second. The data was corrected for bleaching by dividing the intensity obtained in the bleached spot by the intensity of an unbleached area about 10-15 μ m away from the bleaching spot. The background level was subtracted as estimated from the first frame after bleaching. To estimate the diffusion of free CD47, GPMVs were bleached on

the upper pole and recovery curves were fitted using the standard model for free diffusion (Soumpasis, 1983). For the bound membrane segment fluorescent recovery a reaction diffusion model was used (Sprague_et_al.,2004)

$$\begin{aligned}\frac{\partial[L]}{\partial t} &= D_{free}\nabla^2[L] - k_{on}[L][R] + k_{off}[RL] \\ \frac{\partial[R]}{\partial t} &= -k_{on}[L][R] + k_{off}[RL] \\ \frac{\partial[RL]}{\partial t} &= k_{on}[L][R] - k_{off}[RL]\end{aligned}$$

Here [L], [R] and [RL] are the concentrations of free CD47-GFP, surface immobilized SIPRA molecules and bound complexes respectively. ∇^2 has the usual meaning of the Laplace operator and D_{free} , k_{on} and k_{off} are parameters of the model. The data was subsequently fitted to the model using the routine `invlap` (Hollenbeck, 1998) and `nlinfit` (MATLAB 2014a). Note that within the bleached spot there are only about 30-80 CD47 molecules; hence in the first seconds of recovery only a few GFP molecules contribute to the signal. The data is inherently noisy and we found that the recovered absolute values for $[R]k_{on}$ and k_{off} depend significantly on the starting values of the fitting routine. However, the ratio of these rates is robust, in other words $[R]K_{2d}$ is obtained with higher degree of confidence. The error in fitting the individual fluorescent recovery trajectories was estimated following the method of Ref. (Müller_et_al.,2009). The value of the best fit of $[R]k_{on}$ and k_{off} is varied around the best estimate (in the least square sense) until the deviation is found to be outside the bounds set by the χ^2 distribution, effectively giving the 95% confidence intervals.

Fluorescent intensities were quantified either by a line profile on the vesicle equator (to obtain the correlation between GFP and anti-CD47), a line profile on the (x,z) contour in the case of adhering vesicles, both lines were 1 μ m wide, as shown in Figure S1. We used the peak of the resulting intensity distribution as an indicator of dye concentration in the membrane. Using this method one can quantify both the fluorescent intensity in the bound and unbound membrane segments, I_{bound} and I_{free} respectively. We found that the value $[RL] = G \cdot (I_{bound} - I_{free})$ is the most robust way to quantify CD47-SIRP α complex densities using fluorescence confocal microscopy, presumably because small variation or defects in GFP tagging are eliminated this way. Here G is the proportionally factor to convert fluorescent intensities to number density

per membrane area and is determined as described below. Plots of [RL] vs [L]~I_{free} were in general too scattered for detailed analysis and we used these values only as a consistency check as shown in Fig.3C. To assess the CD47 density between RBC and GPMVs we compared the maximum intensity projection at the upper surface of labelled RBC to GPMVs as obtained by high-resolution confocal microscopy (63x1.2 water immersion lens). To convert fluorescent intensities in CD47 concentration, we incubated red blood cells (Fig.S3B) which naturally express CD47 (about 250 molecules/ μm^2 (Tsai_et_al.,2010)), together with the GPMVs and fluorescent CD47 antibodies. The average anti-CD47 fluorescence of RBC cells and co-incubated GPMVs was determined from (x,y) confocal sections of circular shape ($\sim 1\mu\text{m}^2$) at poles and the average number density per area of CD47 molecules on the GPMV population was determined to be about 100 CD47/ μm^2 . The factor G was subsequently assessed from the average CD47 coverage and the average GFP fluorescence intensity in the GPMV population, as determined from line profiles in (x,z) confocal scans on free GPMVs obtained as described above.

Generation of HEK-CD47-GFP Cell Line, Cell culture HEK 293T cells were transduced with a lentivector encoding CD47-GFP and puromycin resistance transgenes. Lentiviral transduction was carried out over 72hrs with a MOI of 5 and followed by puromycin selection (3 $\mu\text{g}/\mu\text{l}$ from gibco by life technologies) for 3 weeks. Cells were then cultured under standard condition in DMEM Media (w/o Phenol Red), 10% FBS and 1% Penicillin-Streptomycin and split every 2-3 days.

Antibody labelling of GPMV, RBC and SIRP α CD47 on GPMVs was labelled by incubation of B6H12 Alexa Fluor 647 Mouse Anti-Human Antibody (BD Biosciences, cat# 561249) for one hour at RT according to the protocol of the manufacturer. RBCs were isolated from a healthy male individual, washed in PBS and incubated in the same conditions as the GPMVs with the antibody. In some experiments, SIRP α was labelled on the glass surface by incubating with rabbit anti-GST Alexa 488 (Invitrogen) at 20 $\mu\text{g}/\text{ml}$ for one hour at RT and subsequent washing.

Phagocytosis assay A549 Cells were opsonized with a Rabbit anti-Human Red Blood Cell RBC Antibody (Rockland, cat# 109-4139 polyclonal, Alvey_et_al.,2017) at final concentration 250 μ g/5ml for one hour at RT. Cells were washed and labelled with the dye PKH26 (Sigma-Aldrich) according to the manufacturers protocol. THP1 cells were left to adhere in standard cell 6-well culture plates in RPMI/PMA media (initial concentration 4 \cdot 10⁵ cells per well) for 48 hours. A549 cells were then added to the wells and incubated at either pH 7.4 or pH 6. After 75 min wells were washed by trypsin and uneaten A549 cells were removed by trypsinization. THP-1 were labelled by incubation with CD11b APC Antibody (Biolegend, cat# 101211 clone M1/70, Alvey_et_al.,2017) at 2ng/ml for one hour at RT. Finally, cells were fixed by incubation with 4% PFA. Imaging was performed using a 10x objective on Leica SP8 system as described below. Images were processed by a Gaussian filter, edges of cells were detected and thresholded to obtain binary images of cells (ImageJ v1.50b). Overlap of the different channels was then calculated per cell.

K3d assay using Red Blood Cells (RBCs) Fresh RBCs were washed and incubated with SIRP α (final concentration 34nM) for one hour at RT in PBS adjusted to pH 7.4 or pH 6. GST was labelled as described before. RBCs were pelleted and unbound protein was washed away. RBCs were then imaged and the mean fluorescence in the center of a RBC was measured in a circle of 6 μ m diameter.

Quantification of CD47 expression during long term acidosis

A549 cells were seeded and grown until confluency for 3 days in full F12 media (supplemented with 25mM HEPES) in the absence of carbon dioxide. Cells were cultured either at pH 7.4 or pH 6. Cells were then detached non-enzymatically, washed and resuspended in PBS supplemented with 5% FBS. CD47 was labeled by incubation for 1h at RT using 3 μ L of Alexa647-human CD47 antibody (BD Biosciences, cat# 561249 clone B6H12, Alvey_et_al.,2017), 0.5 μ L of Hoechst 33342 from Thermofisher (cat# H3570), and 1 μ L of 7-amino-actinomycin D from sigma (Cat# A9400-1MG) per 300 μ l cell suspension. Cells were then washed, resuspended in Flow buffer (5% FBS in PBS), and transferred to flow cytometry

tubes. Cell suspension was analyzed at a flow rate of <1000 cells per second for 1 minute. For Analysis, aggregates were removed from data using Hoechst intensity and FSC. Dead cells, identified as 7ADD+ and low FSC, were also removed from analysis. Quantification of CD47 intensity was recorded as the geometric mean of a give population of cells.

Fluctuation spectroscopy We measured the bending rigidity of the GPMVs by fluctuation analysis of the thermally induced motion of the membrane. Details of the method are published elsewhere(Gracia_et_al.,2010). Experiments were performed on an Axiovert 135 microscope (Zeiss, Germany) using a 40× objective in phase contrast mode. Imaging was done with a fast digital camera HG-100K (Redlake Inc., San Diego, CA) using a mercury lamp HBO W/2 as a light source. We acquired a total of 4000 snapshots per vesicle with exposure time of 200 μs. Only vesicles with clearly visible fluctuations and no visible defects were considered for analysis.

Molecular modeling and coarse-grained simulations of the CD47-SIRPα complex A structural model of the full-length protein CD47 in complex with the SIRPα-GST construct was built using PDB structures 2JJS, 2WNG and 1GTA for the CD47 ectodomain, the SIRPα ectodomain and the GST domain, respectively. The trans-membrane domain of CD47 (comprising residues from 117 to 275) was modeled using EVfold (Hopf_et_al.,2012) and positioned in the membrane environment using the PPM server (Lomize_et_al.,2006). The ectodomains of CD47 and SIRPα as well as the GST domain were next positioned beneath the membrane (see Fig.2a) using VDM (Humphrey_et_al.,1996). The interface between CD47 and SIRPα was taken to be as in the PDB structure 2JJS. The 33-residue peptide segment connecting SIRPα with GST, the 5-residue linker between the two domains of CD47, and the 7-residue loop in the C-terminal Ig-like domain of SIRPα (comprising residues from 288 to 294) were built into the structural model using MODELLER (Fiser_et_al.,2000). The resulting structural model was taken as the initial conformation for molecular simulations. Equilibrium conformations of a single CD47-SIRPα complex were simulated using the coarse-grained model of Kim and Hummer (Kim and Hummer, 2008). The model was adapted to the CD47-SIRPα complex in the following way. Four protein domains were represented as rigid bodies: the trans-membrane domain of CD47, the ectodomain of CD47, the ectodomain of SIRPα, and

the GST domain. The interactions between the individual domains were treated at the residue level and described as in the Kim-Hummer model. A bias potential was applied to 45 inter-domain contacts of the ectodomains of CD47 and SIRP α to ensure the correct binding interface as observed in the crystal structure of the CD47-SIRP α ectodomain complex (PDB code 2JJS). The inter-domain contacts were determined using an overlap criterion (Różycki_et_al.,2014). The bias potential was taken to have a form of the Lennard-Jones potential. The depth of the Lennard-Jones potential was set to 0.67 kT to prevent dissociation of the CD47-SIRP α complex. The GST domain was positioned on a flat substrate with the linker connecting GST to SIRP α oriented away from the substrate, and the trans-membrane domain of CD47 was embedded in a membrane (see Fig.2B). The membrane was assumed to be flat and parallel to the substrate surface. Both the 33-residue peptide segment connecting SIRP α with GST and the 5-residue linker joining the two domains of CD47 were represented as chains of amino-acid beads with appropriate bending, stretching and torsion potentials (Kim and Hummer, 2008). The interactions between the flexible linkers and the rigid domains as well as the interactions between the membrane and the proteins were simulated as in the original model of Kim and Hummer. A harmonic potential was applied between Cys15 (located in the extracellular domain of CD47) and Cys245 (positioned in the trans-membrane domain of CD47) to mimic the disulfide bond.

Monte Carlo (MC) simulations The basic MC moves of the CD47 and SIRP α ectodomains were random rotations and translations in three dimensions. For the trans-membrane domain of CD47, the basic MC moves were translations parallel to the membrane surface and rotations around the axis perpendicular to the membrane surface. For the linker peptides, crank-shaft moves are employed to enhance sampling in addition to local MC moves on each amino-acid bead. The separation between the substrate surface and the membrane was varied in additional MC moves. In the MC simulations, 10^5 configurations taken every 10^3 MC sweeps were generated for analysis. The simulations were performed at room temperature ($T=300$ K). The ectodomains of CD47 and SIRP α were observed to remain in the bound state throughout the simulation runs. The basic MC moves in our simulations of large adhering membrane segments were variations of the local separations l of all membrane patches, and hopping of the harmonic bonds between neighboring patches (Weikl and Lipowsky, 2006).

The bonds are taken to be mobile because positions of CD47-SIRP α complexes in the experiments vary due to binding and unbinding events. Simulations were performed with up to 8×10^7 MC steps per membrane patch.

Distance of membrane-to-substrate in molecular simulations The separation between the membrane and the substrate was identified with the distance measured in the z-direction between the C-terminal residue of the short inter-domain linker in CD47 and the plane at which the GST domain was placed. The histogram of the separations obtained from the MC simulations is shown in Fig.S2. The key quantities obtained from this histogram are the mean value $l_0 = 17.2$ nm, which is the preferred membrane-substrate separation of the complex, and the standard deviation $\sigma = 1.2$ nm, which reflects the flexibility of the complex. Visual inspection of the simulation structures reveals that variations in the separation between membrane and substrate are related mainly to the flexibility of the long linker between SIRP α and GST. Other joints between the rigid domains appear to be relatively stiff. First, in CD47, the trans-membrane domain is connected to the ectodomain by a short linker and by the disulfide bond between Cys15 and Cys245. These two connections, together with steric effects between the protein and the membrane, effectively restrain the orientation of the ectodomain relative to the trans-membrane domain. Second, the relative orientation of the ectodomains of CD47 and SIRP α is restrained by the geometry of their interface. In fact, only small fluctuations around the orientation given by the crystal structure were observed in the simulations.

Competing interests The authors declare no competing or financial interests.

Author contributions Conceptualization: J.S., B.R., C.A., R.L., T.W., R.D., D.D.; Methodology: J.S., B.R., C.A., R.L., T.W., R.D., D.D.; Investigation: J.S., B.R., C.A., T.W.; Data curation: J.S., B.R., C.A., T.W.; Writing - original draft: J.S.; Writing - review & editing: J.S., B.R., C.A., R.L., T.W., R.D., D.D.; Supervision: R.L., T.W., R.D., D.D.; Funding acquisition: B.R., R.L., T.W., R.D., D.D.

Funding Financial support for J.S. from the Deutsche Forschungsgemeinschaft (DFG) via the IRTG-1524 is gratefully acknowledged. B.R. has been supported by the National Science Centre, Poland, grant number 2016/21/B/NZ1/00006. This work is part of the MaxSynBio

consortium which was jointly funded by the Federal Ministry of Education and Research of Germany and the Max Planck Society. Financial support for C.A. and D.D. is from NIH (National Cancer Inst. U54-CA193417, National Heart Lung and Blood Inst. R01-HL124106, R21-HL128187), and a National Science Foundation Materials Science and Engineering Center grant to the University of Pennsylvania.

Acknowledgements Some data and materials and methods in this paper form part of a PhD thesis of Jan Steinkühler (2016, Technischen Universität Berlin).

References

- ALVEY, C. & DISCHER, D. E. 2017. Engineering macrophages to eat cancer: from “marker of self” CD47 and phagocytosis to differentiation. *Journal of Leukocyte Biology*, jlb. 4RI1216-516R.
- ALVEY, C., SPINLER, K., IRIANTO, J., PFEIFER, C., HAYES, B., XIA, Y., CHO, S., DINGAL, D., HSU, J., SMITH, L., TEWARI, M., DISCHER, D.E. 2017. SIRP α -inhibited, marrow-derived macrophages engorge, accumulated, and differentiate in antibody targeted regression of solid tumors. *Current Biology*, 27, 2065-2077.
- BAUER, B., DAVIDSON, M. & ORWAR, O. 2009. Proteomic Analysis of Plasma Membrane Vesicles. *Angewandte Chemie International Edition*, 48, 1656-1659.
- BAUMGART, T., HAMMOND, A. T., SENGUPTA, P., HESS, S. T., HOLOWKA, D. A., BAIRD, B. A. & WEBB, W. W. 2007. Large-scale fluid/fluid phase separation of proteins and lipids in giant plasma membrane vesicles. *Proceedings of the National Academy of Sciences*, 104, 3165-3170.
- BIHR, T., FENZ, S., SACKMANN, E., MERKEL, R., SEIFERT, U., SENGUPTA, K. & SMITH, A.-S. 2014. Association Rates of Membrane-Coupled Cell Adhesion Molecules. *Biophysical Journal*, 107, L33-L36.
- BISWAS, A., ALEX, A. & SINHA, B. 2017. Mapping Cell Membrane Fluctuations Reveals Their Active Regulation and Transient Heterogeneities. *Biophysical journal*, 113, 1768-1781.
- BOURA, E., RÓŻYCKI, B., CHUNG, HOI S., HERRICK, DAWN Z., CANAGARAJAH, B., CAFISO, DAVID S., EATON, WILLIAM A., HUMMER, G. & HURLEY, JAMES H. 2012. Solution Structure of the ESCRT-I and -II Supercomplex: Implications for Membrane Budding and Scission. *Structure*, 20, 874-886.
- BOURA, E., RÓŻYCKI, B., HERRICK, D. Z., CHUNG, H. S., VECER, J., EATON, W. A., CAFISO, D. S., HUMMER, G. & HURLEY, J. H. 2011. Solution structure of the ESCRT-I complex by small-angle X-ray scattering, EPR, and FRET spectroscopy. *Proceedings of the National Academy of Sciences*, 108, 9437-9442.
- CHAN, Y.-H. M., LENZ, P. & BOXER, S. G. 2007. Kinetics of DNA-mediated docking reactions between vesicles tethered to supported lipid bilayers. *Proceedings of the National Academy of Sciences*, 104, 18913-18918.
- FENZ, S. F. & SENGUPTA, K. 2012. Giant vesicles as cell models. *Integrative Biology*, 4, 982-995.
- FISER, A., DO, R. K. & SALI, A. 2000. Modeling of loops in protein structures. *Protein Science : A Publication of the Protein Society*, 9, 1753-1773.
- FRANCIS, D. M., RÓŻYCKI, B., TORTAJADA, A., HUMMER, G., PETI, W. & PAGE, R. 2011. Resting and Active States of the ERK2:HePTP Complex. *Journal of the American Chemical Society*, 133, 17138-17141.
- GRACIA, R. S., BEZLYEPKINA, N., KNORR, R. L., LIPOWSKY, R. & DIMOVA, R. 2010. Effect of cholesterol on the rigidity of saturated and unsaturated membranes: fluctuation and electrodeformation analysis of giant vesicles. *Soft Matter*, 6, 1472-1482.
- HOLLENBECK, K. J. 1998. INVLAP.M: A matlab function for numerical inversion of Laplace transforms by the de Hoog algorithm.
- HOPF, THOMAS A., COLWELL, LUCY J., SHERIDAN, R., ROST, B., SANDER, C. & MARKS, DEBORA S. 2012. Three-Dimensional Structures of Membrane Proteins from Genomic Sequencing. *Cell*, 149, 1607-1621.

- HU, J., LIPOWSKY, R. & WEIKL, T. R. 2013. Binding constants of membrane-anchored receptors and ligands depend strongly on the nanoscale roughness of membranes. *Proceedings of the National Academy of Sciences*, 110, 15283-15288.
- HUMPHREY, W., DALKE, A. & SCHULTEN, K. 1996. VMD: visual molecular dynamics. *Journal of molecular graphics*, 14, 33-38.
- HUPPA, J. B., AXMANN, M., MORTELMAYER, M. A., LILLEMEIER, B. F., NEWELL, E. W., BRAMESHUBER, M., KLEIN, L. O., SCHUTZ, G. J. & DAVIS, M. M. 2010. TCR-peptide-MHC interactions in situ show accelerated kinetics and increased affinity. *Nature*, 463, 963-967.
- KIM, Y. C. & HUMMER, G. 2008. Coarse-grained Models for Simulations of Multiprotein Complexes: Application to Ubiquitin Binding. *Journal of Molecular Biology*, 375, 1416-1433.
- KROBATH, H., RÓŻYCKI, B., LIPOWSKY, R. & WEIKL, T. R. 2009. Binding cooperativity of membrane adhesion receptors. *Soft Matter*, 5, 3354-3361.
- LIPOWSKY, R. 1991. The conformation of membranes. *Nature*, 349, 475-481.
- LIPOWSKY, R. 1995. Generic interactions of flexible membranes. *Handbook of biological physics*, 1, 521-602.
- LOMIZE, M. A., LOMIZE, A. L., POGOZHEVA, I. D. & MOSBERG, H. I. 2006. OPM: Orientations of Proteins in Membranes database. *Bioinformatics*, 22, 623-625.
- MONZEL, C., SCHMIDT, D., KLEUSCH, C., KIRCHENBÜCHLER, D., SEIFERT, U., SMITH, A. S., SENGUPTA, K. & MERKEL, R. 2015. Measuring fast stochastic displacements of bio-membranes with dynamic optical displacement spectroscopy. *Nature Communications*, 6, 8162.
- MORONE, N., FUJIWARA, T., MURASE, K., KASAI, R. S., IKE, H., YUASA, S., USUKURA, J. & KUSUMI, A. 2006. Three-dimensional reconstruction of the membrane skeleton at the plasma membrane interface by electron tomography. *J Cell Biol*, 174, 851-862.
- MÜLLER, K. P., ERDEL, F., CAUDRON-HERGER, M., MARTH, C., FODOR, B. D., RICHTER, M., SCARANARO, M., BEAUDOUIN, J., WACHSMUTH, M. & RIPPE, K. 2009. Multiscale Analysis of Dynamics and Interactions of Heterochromatin Protein 1 by Fluorescence Fluctuation Microscopy. *Biophysical Journal*, 97, 2876-2885.
- OLDENBORG, P.-A., ZHELEZNYAK, A., FANG, Y.-F., LAGENAUR, C. F., GRESHAM, H. D. & LINDBERG, F. P. 2000. Role of CD47 as a marker of self on red blood cells. *Science*, 288, 2051-2054.
- RÓŻYCKI, B., MIODUSZEWSKI, Ł. & CIEPLAK, M. 2014. Unbinding and unfolding of adhesion protein complexes through stretching: Interplay between shear and tensile mechanical clamps. *Proteins: Structure, Function, and Bioinformatics*, 82, 3144-3153.
- SEIFFERT, M., CANT, C., CHEN, Z., RAPPOLD, I., BRUGGER, W., KANZ, L., BROWN, E. J., ULLRICH, A. & BÜHRING, H.-J. 1999. Human Signal-Regulatory Protein Is Expressed on Normal, But Not on Subsets of Leukemic Myeloid Cells and Mediates Cellular Adhesion Involving Its Counterreceptor CD47. *Blood*, 94, 3633-3643.
- SEZGIN, E., KAISER, H.-J., BAUMGART, T., SCHWILLE, P., SIMONS, K. & LEVENTAL, I. 2012. Elucidating membrane structure and protein behavior using giant plasma membrane vesicles. *Nat. Protocols*, 7, 1042-1051.

- SOSALE, N. G., ROUHIPARKOUHI, T., BRADSHAW, A. M., DIMOVA, R., LIPOWSKY, R. & DISCHER, D. E. 2015a. Cell rigidity and shape override CD47's "self"-signaling in phagocytosis by hyperactivating myosin-II. *Blood*, 125, 542-552.
- SOSALE, N. G., SPINLER, K. R., ALVEY, C. & DISCHER, D. E. 2015b. Macrophage engulfment of a cell or nanoparticle is regulated by unavoidable opsonization, a species-specific 'Marker of Self' CD47, and target physical properties. *Current Opinion in Immunology*, 35, 107-112.
- SOUMPASIS, D. M. 1983. Theoretical analysis of fluorescence photobleaching recovery experiments. *Biophysical Journal*, 41, 95-97.
- SPRAGUE, B. L., PEGO, R. L., STAVREVA, D. A. & MCNALLY, J. G. 2004. Analysis of Binding Reactions by Fluorescence Recovery after Photobleaching. *Biophysical Journal*, 86, 3473-3495.
- SUBRAMANIAN, S., BODER, E. T. & DISCHER, D. E. 2007. Phylogenetic Divergence of CD47 Interactions with Human Signal Regulatory Protein α Reveals Locus of Species Specificity: IMPLICATIONS FOR THE BINDING SITE. *Journal of Biological Chemistry*, 282, 1805-1818.
- SUBRAMANIAN, S., PARTHASARATHY, R., SEN, S., BODER, E. T. & DISCHER, D. E. 2006. Species- and cell type-specific interactions between CD47 and human SIRP α . *Blood*, 107, 2548-2556.
- TANNOCK, I. F. & ROTIN, D. 1989. Acid pH in Tumors and Its Potential for Therapeutic Exploitation. *Cancer Research*, 49, 4373-4384.
- TOLENTINO, T. P., WU, J., ZARNITSYNA, V. I., FANG, Y., DUSTIN, M. L. & ZHU, C. 2008. Measuring Diffusion and Binding Kinetics by Contact Area FRAP. *Biophysical Journal*, 95, 920-930.
- TSAI, R. K., RODRIGUEZ, P. L. & DISCHER, D. E. 2010. Self inhibition of phagocytosis: the affinity of 'Marker of Self' CD47 for SIRP α dictates potency of inhibition but only at low expression levels. *Blood cells, molecules & diseases*, 45, 67-74.
- TURLIER, H., FEDOSOV, D. A., AUDOLY, B., AUTH, T., GOV, N. S., SYKES, C., JOANNY, J. F., GOMPPER, G. & BETZ, T. 2016. Equilibrium physics breakdown reveals the active nature of red blood cell flickering. *Nat Phys*, 12, 513-519.
- VEATCH, S. L., CICUTA, P., SENGUPTA, P., HONERKAMP-SMITH, A., HOLOWKA, D. & BAIRD, B. 2008. Critical fluctuations in plasma membrane vesicles. *ACS chemical biology*, 3, 287-293.
- VERNON-WILSON, E. F., KEE, W.-J., WILLIS, A. C., BARCLAY, A. N., SIMMONS, D. L. & BROWN, M. H. 2000. CD47 is a ligand for rat macrophage membrane signal regulatory protein SIRP (OX41) and human SIRP α 1. *European Journal of Immunology*, 30, 2130-2137.
- WEIKL, T. R., ASFAW, M., KROBATH, H., RÓŻYCKI, B., LIPOWSKY, R. 2009. Adhesion of membranes via receptor-ligand complexes: Domain formation, binding cooperativity, and active processes. *Soft Matter*, 5, 3213-3224.
- WEIKL, T. R. & LIPOWSKY, R. 2006. Membrane adhesion and domain formation. *Advances in Planar Lipid Bilayers and Liposomes*, 5, 63-127.
- XU, G.-K., HU, J., LIPOWSKY, R. & WEIKL, T. R. 2015. Binding constants of membrane-anchored receptors and ligands: A general theory corroborated by Monte Carlo simulations. *The Journal of chemical physics*, 143, 243136.
- ZHU, D.-M., DUSTIN, M. L., CAIRO, C. W. & GOLAN, D. E. 2007. Analysis of Two-Dimensional Dissociation Constant of Laterally Mobile Cell Adhesion Molecules. *Biophysical Journal*, 92, 1022-1034.

Figures

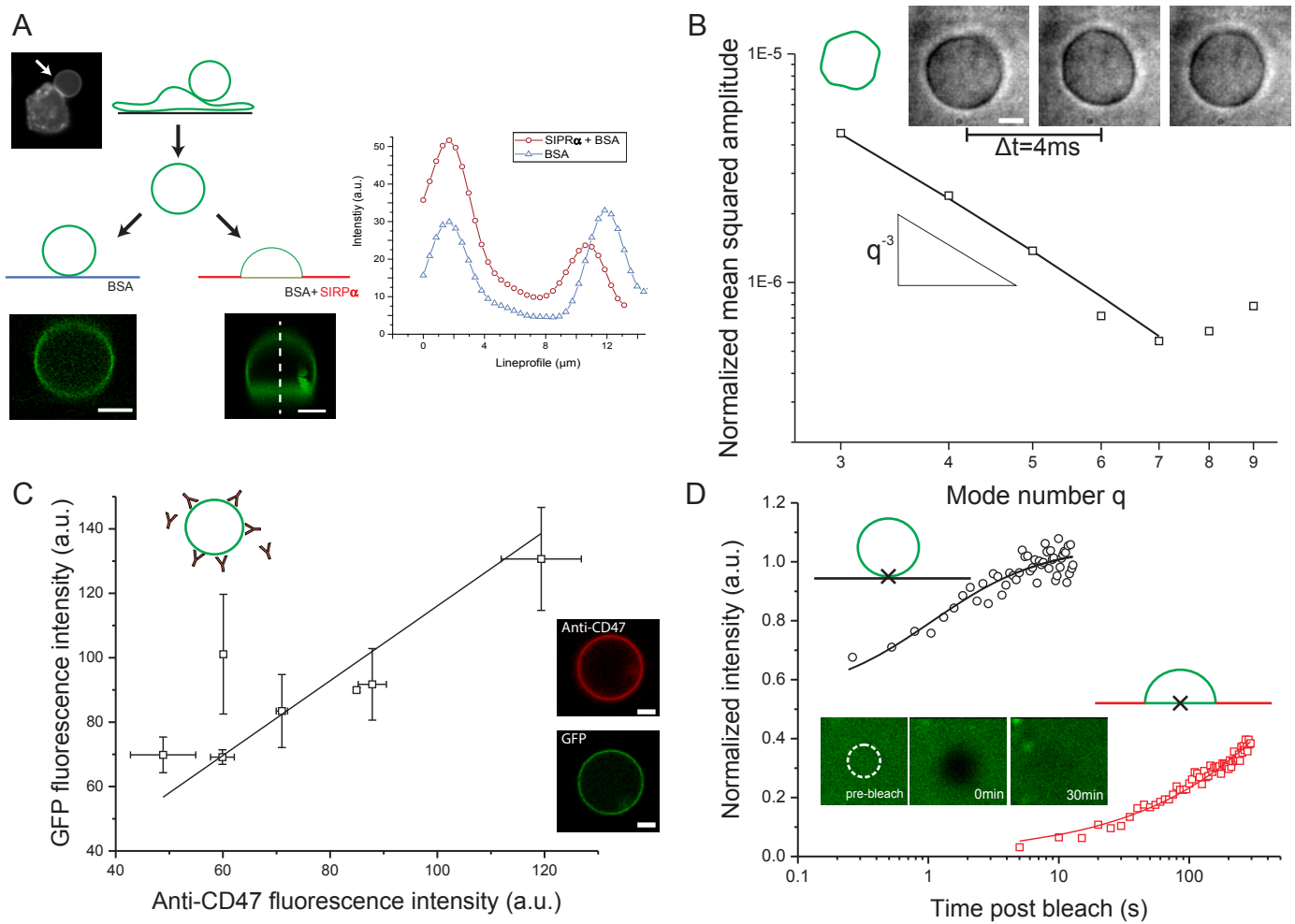


Figure 1: GPMV characterization and CD47-GFP diffusion. (a) GPMV formation from CD47-GFP expressing HEK cells. Left: Epi-fluorescence image of a cell with an attached GPMV (arrow). Right: Confocal microscopy z-stacks of a free GPMV on a BSA-coated coverslip (left) or an adherent GPMV on a SIRP α -coated coverslip (right). Representative fluorescent intensity traces quantified from image stacks. Lines are guides to the eye. (b) Fluctuation analyses of GPMVs are compatible with elastic sheet model of bending rigidity $\kappa \approx 10k_B T \pm 3k_B T$ S.D. Inset: phase contrast images of thermal fluctuations. Low exposure times of 200 μ s and 4000 images per vesicle avoid artefacts from averaging fast fluctuations. (c) Anti-CD47 and GFP signals correlate in confocal microscopy: $y = 1.2x$ ($R^2 = 0.98$). Each datapoint corresponds to measurement of an individual GPMV in at least two independent

experiments. (d) Representative recovery curve in FRAP of CD47-GFP: on 1) unbound membrane segments (black circles) with fit to free diffusion model, and 2) after bleaching the adhering membrane segment (red squares) with fit to adhesion model. Data was normalized to the average fluorescent intensity of the unbleached area before application of the bleaching pulse. Note the logarithmic time scale. Crosses indicate bleached location on vesicles. Inset images: Bleached CD47-GFP shows full recovery on longer timescales. White circle indicates bleached area of 1 μ m in diameter. Other scalebars 5 μ m.

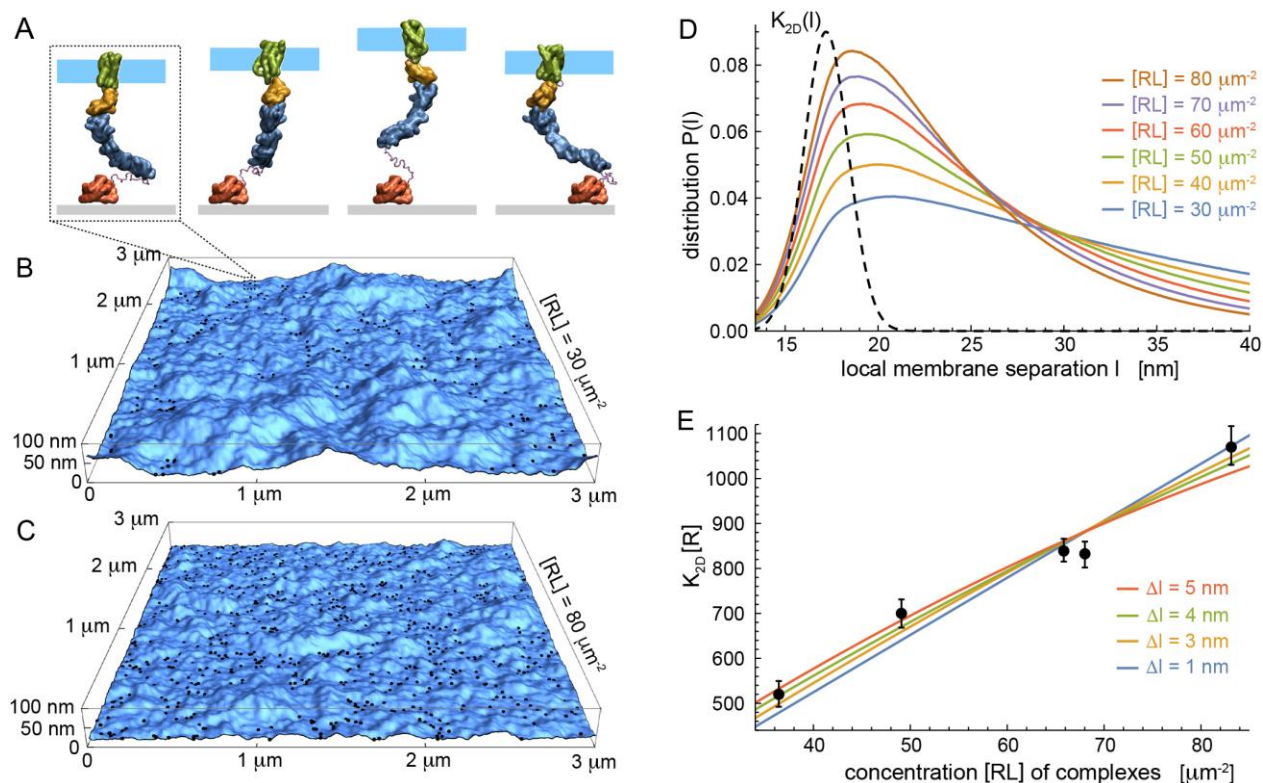


Figure 2: Multiscale modeling of experiments clarify interactions. (a) Binding constant K_{2D} as a function of complex concentration $[RL]$ from experiments (data points) and modeling (lines) for different values Δl of repulsive membrane-substrate interactions. Modeling is based on Eq.(1), with fit values $K_{max}=(956\pm 24)/[R]$, $(470\pm 10)/[R]$, $(378\pm 8)/[R]$, and $(326\pm 8)/[R]$ for $\Delta l=1, 3, 4, 5$ nm, respectively. Binding constant K_{2D} has units of concentration $[R]$ of unbound $SIRP\alpha$. Error bars indicate 95% confidence intervals for fitting the reaction-diffusion model, \pm standard error (SEM). Each datapoint corresponds to measurement of an individual GPMV in at least two independent experiments. (b) Simulation snapshots of coarse-grained CD47-SIRP α complex. Separation between fluid membrane patch (cyan) and substrate (grey) varies in simulations mainly because of conformational changes of the unstructured linker that covalently connects extracellular SIRP α domain (blue) to substrate-bound GST (red). (c, d) Snapshots of adhering membranes with area $3\times 3\mu m^2$ for respective concentrations $[RL]=30, 80\mu m^{-2}$ of CD47-SIRP α complexes at $\Delta l=4$ nm. Black dots indicate

complexes varied in their positions. (e) Distributions $P(l)$ for local separation between membrane and substrate obtained from averaging over many membrane snapshots for various $[RL]$. Dashed black line represents $K_{2D}(l)$ (arbitrary units).

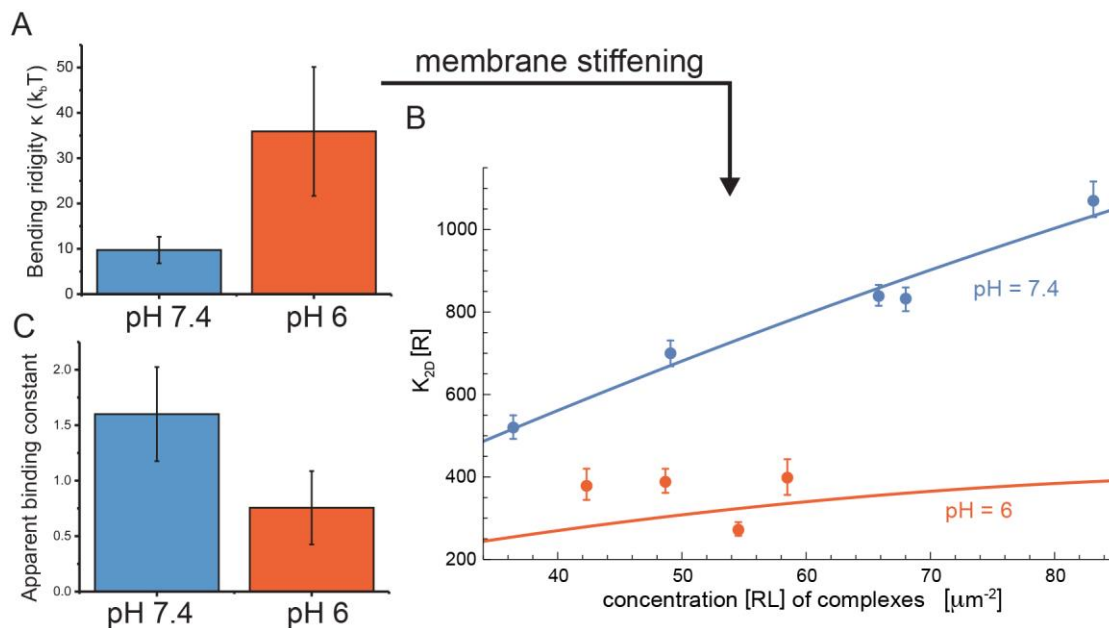


Figure 3: Acidosis conditions (pH=6) affect membrane flexibility and interactions. (a) Membrane fluctuations reveal 3.6-fold stiffening of GPMV membranes upon pH shift (n=9 GPMVs per condition) (b) Binding constant K_{2D} as a function of the complex concentration [RL] from experiments (datapoints) and simulation (lines) at pH=7.4 and 6, respectively, for the parameter value $\Delta l=4$ nm of the repulsive membrane-substrate interactions. Model uses measured bending rigidities $\kappa=10$ k_BT at pH=7.4 and $\kappa=40$ k_BT at pH=6 and varies the maximal binding constant K_{max} in Eq.(1). At pH=7.4, the best-fit $K_{\text{max}}=(378\pm 8)/[R]$ ($R^2=0.997$) for $\Delta l=4$ nm (see Fig.2(d)). At pH=6, $K_{\text{max}}=(74\pm 8)/[R]$ ($R^2=0.997$) for $\Delta l=4$ nm, and the best-fit value depends weakly on Δl . Error bars are 95% confidence intervals of the fit to the reaction-diffusion model (\pm SEM). Each datapoint corresponds to measurement of an individual GPMV in at least two independent experiments. (c) Apparent binding constant at low CD47 ($\sim 40\pm 10/\mu\text{m}^2$) as independently obtained from fluorescence (Fig.S1; Supplemental Material and Methods) is consistent with FRAP in panel-b (n=5 GPMVs per condition). Differences between distributions are significant ($p<0.05$, t-test).

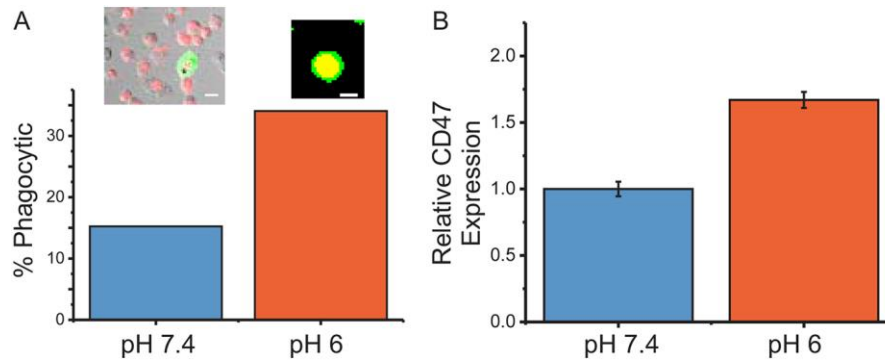


Figure 4: Phagocytosis and CD47 levels change with acidosis. (a) Phagocytic uptake assay of opsonized A549 (red in insets) cells by THP-1 macrophages (green). Yellow indicates overlapping cells, and full overlap indicates completed phagocytosis. Shift to pH 6 increases such engulfment. Left inset shows phase contrast images overlaid with fluorescence. Scalebar=10 μ m. Data from two independent experiments (n=90 cells for pH=7, n=47 for pH=6). (b) CD47 levels increase on viable A549 cells under acidosis conditions. Experiment was performed with three technical replicates. Error bars: \pm SEM. Differences between distributions are significant ($p < 0.05$, t-test).

Supplemental Figures

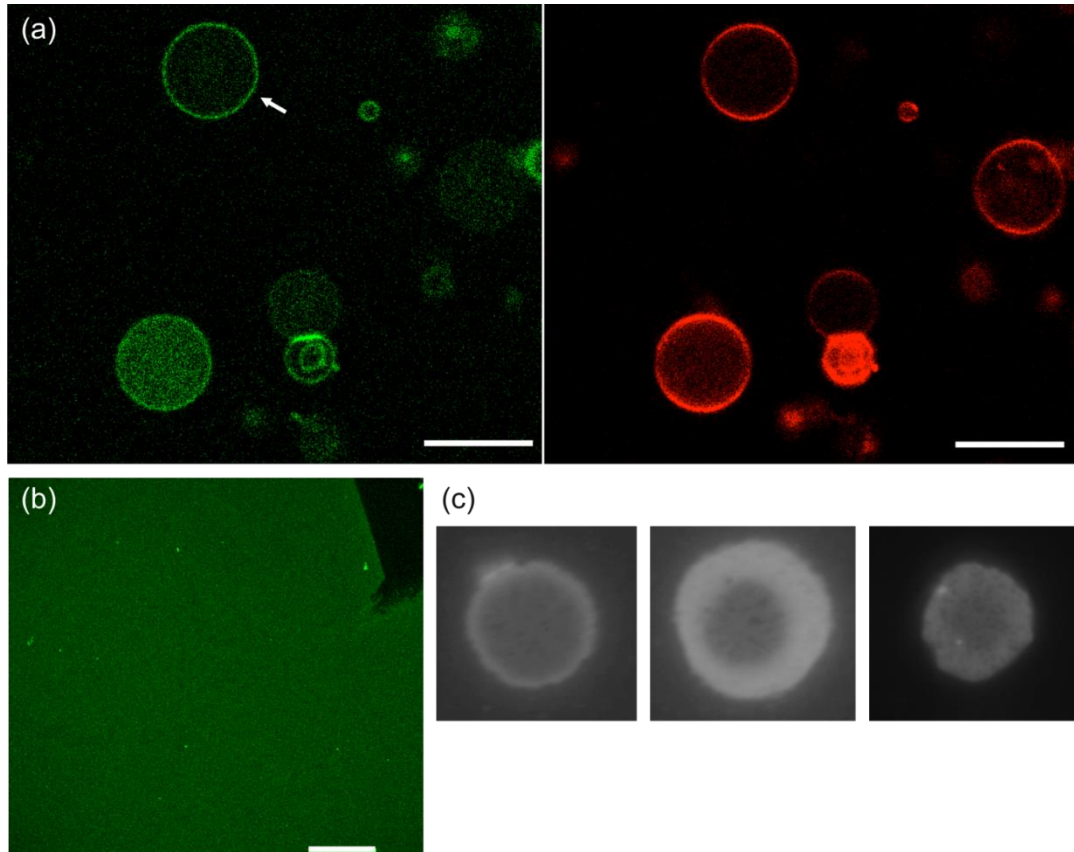


Fig. S1. (a) Confocal images of isolated GPMVs. Left: GFP labelled CD47. Right: Membrane marker DiIC18. The arrow indicates a typical vesicle selected for experiments. Scale bars 10 μ m (b) Anti-GST staining of SIRP α absorbed on a glass slide. The black region is a scratch with a pipette tip to estimate the background level. By fluorescence measurements and comparison to the known density of fluorophores on RBC incubated with free SIRP α , we estimate the SIRP α density to roughly $[R_0] \approx 4000$ molecules/ μ m². This estimate is consistent with E-selectin densities obtained by physisorption on glass slides under similar conditions(1) and in the same order of magnitude as SIRP α layers obtained on plastic surfaces (2). The density is below the maximum packing density of a SIRP α monolayer and we can expect that BSA, which is used for blocking uncovered glass surface, fill the gaps between individual SIRP α molecules. Scale bar 60 μ m. (c) CD47-GFP TIRF micrographs of the adhering GPMV segment on a SIRP α labeled glass surface. Micrographs were acquired on three different GPMVs during the first 5-20 minutes after initial GPMV adhesion. The ring-like CD47-GFP patterns equilibrated over time to a homogenous fluorescence signal. All further experiments were conducted on equilibrated, homogenous adhesion segments. Adhesion segments were typically about 10 μ m in diameter.

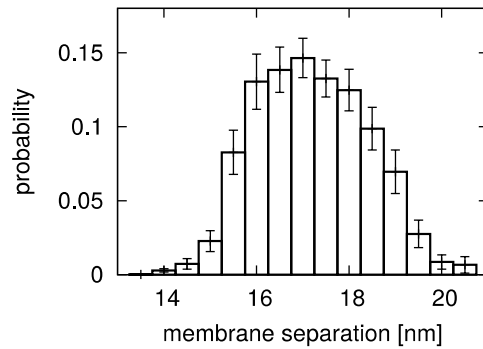


Fig. S2 Probability distribution of membrane-substrate distance obtained from simulations of the coarse-grained CD47-SIRP α complex.

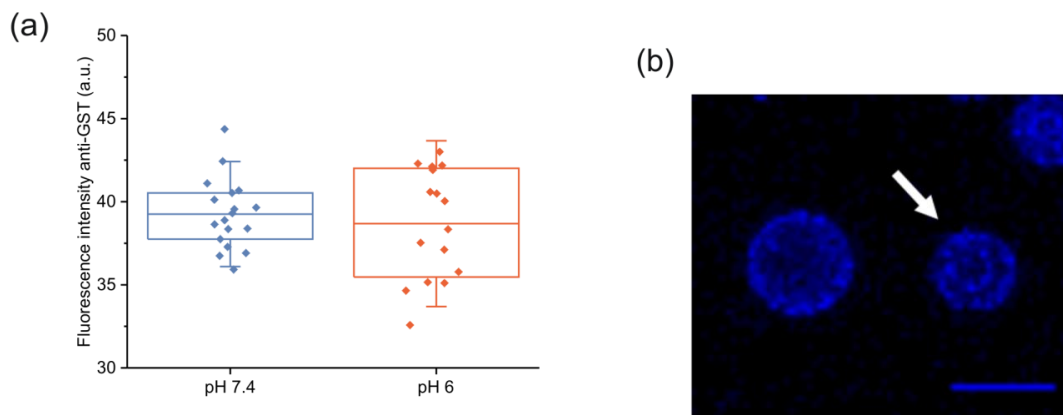


Fig. S3. (a) Binding of (water soluble) GST-SIRP α to RBC showed no significant effect of shift from pH=7.4 to pH=6 on K3d binding affinity. (b) Incubation of red blood cells (RBCs) together with GPMVs and fluorescent anti-CD47 in order to estimate the CD47 concentration on GPMV's. Arrow indicates RBC. Scale bar 10 μ m

1. Lorz, B. G., A.-S. Smith, C. Gege, and E. Sackmann. 2007. Adhesion of Giant Vesicles Mediated by Weak Binding of Sialyl-LewisX to E-Selectin in the Presence of Repelling Poly(ethylene glycol) Molecules. *Langmuir* 23:12293-12300.
2. Subramanian, S., R. Parthasarathy, S. Sen, E. T. Boder, and D. E. Discher. 2006. Species- and cell type-specific interactions between CD47 and human SIRP α . *Blood* 107:2548-2556.